



The effect of geomagnetic storms on the total electron content over the low latitude Saudi Arab region: a focus on St. Patrick's Day storm

Sunil Kumar Sharma¹ · Arun Kumar Singh² · Sampad Kumar Panda³ · Sameh S. Ahmed^{4,5}

Received: 14 December 2019 / Accepted: 11 February 2020
© Springer Nature B.V. 2020

Abstract The present paper investigates the ionospheric response to the severe geomagnetic storms on St. Patrick's Day (17 March 2015) and the strong geomagnetic storm (7 October 2015) over the low latitude Saudi Arab region. The GNSS-TEC observations over low latitude RASH station (28°29'N, 34°46'E) in Saudi Arab confirms that the spatial-temporal alterations over the region not only solely depends on the low latitude electrodynamics but also relies on the high and mid electrodynamics. During the St. Patrick's Day storm, minimum Dst has reached to -223 nT with AE enhancement up to 2215 nT and VTEC values shown maximum enhancement of 250.16% with comparison to average quiet days VTEC, which is known as the positive effect of geomagnetic storm. The positive response of the VTEC has been observed over the region due to the coexistence of Prompt penetration electric field (PPEF) with the prevailed long duration Disturbance dynamo electric field (DDEF). The F2 layer gets uplifted with the enhanced fountain effect through the equatorial $E \times B$ drift, which is observed with the enhancement in hmF2 and enhancement in O/N2 ratio. Concerning the strong geomagnetic storm event on 7 October 2015, minimum Dst has reached to -124 nT with

AE enhancement up to 1209.30 nT and VTEC values shown minimum decrement of -72.14% as compared to the average quiet days VTEC, which is known as the negative effect of geomagnetic storm. The negative response of VTEC has been observed during the main phase of the storm, possibly due to the consequences of suppressed equatorial ionization anomaly (EIA) over the observatory station. The negative response has been described by the downward movement of F2 layer with apparent reduction in hmF2 and depletion in O/N2 ratio over the low latitude region. The results during the storm period also demonstrate that the intensity of amplitude scintillation is enhanced over the low latitude region whose magnitude depends on the severity of the geomagnetic storm.

Keywords St. Patrick's Day storm · Space weather · Low latitude region · Total electron content · Scintillation

1 Introduction

The electrical, neutral and electrodynamic coupling between the magnetosphere and the high latitude ionosphere during the episode of geomagnetic storm has proven its significant impact on the equatorial and lower latitude ionospheric electrodynamics. In brief, the particles precipitation and magnetospheric convection are primary source of electrodynamic process on high latitude ionosphere (Huang et al. 2007; Kikuchi et al. 2008; Kikuchi and Hashimoto 2016). The increased energy and momentum deposition in the high latitude region due to the particle precipitation and joule heating subsequently changes the plasma density and can cause drifts over the equatorial ionosphere. The currents at high latitude region transfer the energy to the neutral gases by

✉ S.K. Sharma
s.sharma@mu.edu.sa

¹ College of Computer and Information Sciences, Majmaah University, Majmaah 11952, Saudi Arabia
² University of Allahabad, Old Katra, Prayagraj, Uttar Pradesh 211002, India
³ K L Deemed to be University, Koneru Lakshmaiah Education Foundation, Guntur, Andhra Pradesh 522502, India
⁴ Mining and Metallurgical Engineering Department, Faculty of Engineering, Assiut University, Assiut 71516, Egypt
⁵ Department of Civil and Environmental Engineering, College of Engineering, Majmaah University, Majmaah 11952, Kingdom of Saudi Arabia

the joule heating process. The ampere force works as an external force to move the neutral winds from polar region to equatorial and low latitudes. The equatorward thermospheric winds around F-layer height is the results of momentum force and joule heating at high latitude region (Richmond and Roble 1979). These thermospheric winds return to E-layer altitudes in the vicinity of magnetic equator, which were flowing from high latitude to equatorial region. The uplifting of F2 layer is the result of these thermospheric winds, which makes foF2 and hmF2 enhancement in day time. They also enhance the total electron content and responsible for the global atmospheric composition changes (Goncharenko et al. 2007; Lu et al. 2008; Ansari et al. 2019; Reddybattula et al. 2019).

There are two major drivers of low latitude electrodynamics during the progress of geomagnetic storm across the low latitude zone on both the hemisphere. The first one is the disturbance dynamo electric field (DDEF) which is characterized by a long-lasting effect (Araki et al. 1985; Blanc and Richmond 1980) on the plasma distribution, and second is the prompt penetration electric field (PPEF) that is abrupt and sustains for relatively shorter duration (Kikuchi and Araki 1979; Koba et al. 2000; Yamazaki and Kosch 2015). A dawn to dusk electric field gets generated at high latitudes due to the changes in the direction of interplanetary magnetic field (IMF-Bz) i.e. when the IMF-Bz turns southward from northward direction. Thus it develops undershielding at the low-latitude ionosphere (Somayajulu et al. 1987; Huang et al. 2005). The propagation of hydromagnetic waves towards the low latitude region from the magnetosphere is the result of the undershielding electric field mapping towards the low latitude and equatorial region during the main phase of the geomagnetic storm (Kikuchi 1986).

The St. Patrick's Day storm on 17 March 2015 is the strongest event of solar cycle-24 (Dst index -223 nT). The origin, development and ionospheric effects of this particular geomagnetic storm have been discussed by many researchers around different part of the globe (Sahai et al. 2011; De Jesus et al. 2012; Seif et al. 2012; Panda et al. 2014; Astafyeva et al. 2015; Zhou et al. 2016; Kil et al. 2016; Chen et al. 2016; Borries et al. 2016; Hairston et al. 2016; Reddybattula and Panda 2019). These exploit the unique and new characteristics of the equatorial, lower, and higher latitude ionosphere at different longitudes during this specific event. There are also studies on equatorial plasma bubbles (EPBs) during the St. Patrick's event reporting depletion in the EPBs growth during the post-sunset hours but enhancements during the post-midnight hours during the storm day (Carter et al. 2016).

The present study exploits the recorded GNSS data at the RASH station in Saudi Arabia to investigate the low latitude ionospheric response to the severe storm event during the St. Patrick's Day (17 March 2015) and the strong storm on

7 October 2015. The work also includes the global behavior of Ionospheric F-layer parameters (NmF2, hmF2) and neutral O/N2 ratio supporting compositional changes during the storm period. Ground based Global Navigation Satellite System (GNSS) derived TEC data and the global distributions of ionospheric parameters have been utilized to analyze the storm-time ionospheric abnormalities during two different events with varied seasonal characteristics. Further, the work includes analyzing the severity of scintillations due to the plasma gradients in the equatorial and low latitude ionosphere. There are recent investigations on the diurnal, monthly and seasonal variations of ionospheric TEC and performance analysis of International Reference Ionosphere (IRI) model over Bahrain, falling the close vicinity of Saudi Arabia (Sharma et al. 2018; Sharma 2019). However, to the best of our knowledge, although there are several papers on large scale global as well as regional storm-time ionospheric characteristics, there are hardly any works on investigating the St. Patrick's Day storm effect Saudi Arabian low latitude ionosphere due to unavailability of sufficient data. In the present study, a new set of database has been used to study the TEC variation over the region.

The second section describes the data and analysis method used to extract the VTEC data from GNSS observables. Third section presents the results and discussion part of the work including the effect of geomagnetic storm on St. Patrick's Day and that of 7 October 2015. It also includes the scintillation occurred during both geomagnetic storms. In section four, the conclusions have been drawn from the analysis of the results.

2 Data and analysis

This work has been performed using the dual frequency ground-based GNSS observations at RASH station ($28^{\circ}29'N$, $34^{\circ}46'E$) in Saudi Arabia. The Rinex GPS-TEC program developed by Gopi Seemala has been used for determining the vertical TEC (VTEC) from the differential carrier phase and pseudorange observations (Seemala and Valladares 2011). This GNSS-TEC analysis program uses the differential code biases (DCBs) and ephemeris data for estimating the slant TEC. The smoothing of GNSS pseudorange by the method of carrier phase labeling helps to remove the noises in the pseudorange TEC data. The following equation (1) has been used to calculate the STEC along the satellite receiver and it also includes the instrumental bias (B).

$$\text{STEC} = \text{VTEC} + B \quad (1)$$

So STEC can be converted into VTEC after removal of instrument biases. The STEC is converted to VTEC using

Eq. (2):

$$\text{VTEC} = \text{STEC} \times \left(1 - \left(\frac{R_E \cos(\alpha)}{R_E + h_{\max}} \right) \right)^{1/2} \quad (2)$$

Where, R_E represents the radius of the earth, α is the elevation cutoff and h_{\max} is the altitude of ionospheric pierce point (IPP) that is considered to be at 350 km. The elevation cutoff is chosen greater than 20° to avoid the error due to multipath, tropospheric effects, and changes in the geometry of satellites.

The percentage variation in VTEC has been calculated to show the maximum and minimum changes in VTEC values during the storms days. The percentage VTEC is the difference between the storm days VTEC and average of 10 quiet days of the respective month. The %VTEC is calculated from Eq. (3):

$$\% \text{VTEC} = (\text{VTEC}_{\text{SD}} - \text{VTEC}_{\text{AQ}}) / \text{VTEC}_{\text{SD}} * 100 \quad (3)$$

Where, VTEC_{SD} is the VTEC during storm day and VTEC_{AQ} are Average 10 quiet days VTEC.

To study the response of ionosphere during the geomagnetic storms, top two geomagnetic storms of year 2015 (based on the geomagnetic storm time index, Dst) have been chosen i.e., 17 March 2015 (St. Patrick's Day storm) and 7 October 2015. The background geophysical conditions data (IMF-Bz, Proton density, solar wind speed and interplanetary electric field-Ey, Kp index, and AE index) have been downloaded from the OMNI Web server (<https://omniweb.gsfc.nasa.gov/form/dx1.html>). The Sym-H data has been downloaded from the World Data Center for Geomagnetism, Kyoto website (<http://wdc.kugi.kyoto-u.ac.jp/aeasy/index.html>). The global distribution of the O/N2 ratio graphs has been downloaded from the integrated space weather analysis system (ISWA) <https://iswa.ccmc.gsfc.nasa.gov>. The auto scale data of F2 layer critical frequency (foF2), its height (hmF2), and minimum virtual height of F2 layer (hF2) have been downloaded from the Global Ionosphere Radio Observatory (GIRO) archives <http://giro.uml.edu/drift-data.html>. In this case, due to unavailability of direct observation of ionospheric F layer parameters from collocated or nearby ionosonde/digisonde/incoherent scatter radar observation, the digisonde parameters at an approximate equivalent latitude station Athens (38°N , 23°E) has been considered in this study to support the GNSS TEC analysis. The location of GPS TEC observatory station (RASH) and Ionosonde observatory station (Athens) is shown in Fig. 1.

3 Results and discussion

We tried to investigate the response of low latitude ionosphere over the RASH station ($28^\circ 29'\text{N}$, $34^\circ 46'\text{E}$) in Saudi



Fig. 1 The graph shows the location of the GPS measurement RASH station ($28^\circ 29'\text{N}$, $34^\circ 46'\text{E}$) and Ionosonde measurement Athens station (38°N , 23°E)

Arab to the occurrence of geomagnetic storms. The study has been divided into three different parts. The first part describes the Positive storm effect of St. Patrick's Day event (17th March 2015) on the diurnal TEC variation over the observatory station. Second part describes the negative response of ionospheric TEC due to the occurrence of strong storm on 7th October 2015. Third part describes the scintillation observed during both geomagnetic storms and their inter comparisons on the basis of intensity of the scintillation.

Figure 2 describes the diurnal variation of VTEC and Averaged Quiet days VTEC with standard deviation during the storm days 17 March 2015 and 7 October 2015 in the top panel and the percentage variation in VTEC on storms days as compared to the averaged quiet days VTEC in the below panel. It can be seen from Fig. 2 that the VTEC is 250.16% higher as compared to the average ten quiet days VTEC of March month during the geomagnetic storm occurred on 17 March, which leads to positive response of storm, while during the storm on 7 October 2015, VTEC is 72.14% lower as compared to ten quiet days of October month, which is indication of negative response of the storm. The initial, main and recovery phase of storms has been discussed in Sects. 3.1 and 3.2 by observing the variation of VTEC during precursor and successor day of the storm. The Root Mean Square Error (RMSE) is calculated between VTEC values and monthly median values are 6.32 and 7.96 during 17 March 2015 and 7 October 2015 respectively.

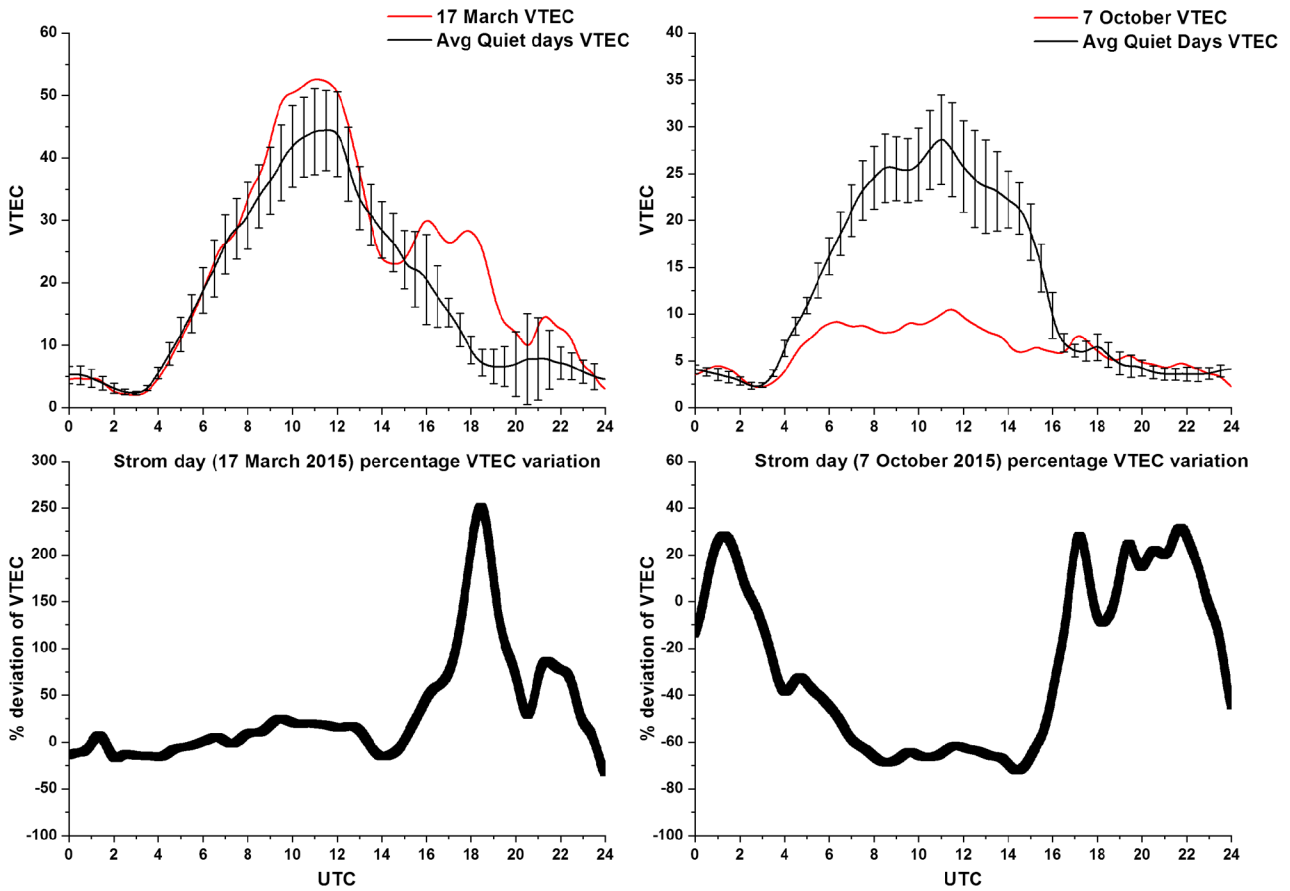


Fig. 2 Diurnal variation of VTEC and averaged ten quiet days VTEC with its standard deviation during the 17 March 2015 and 7 October 2015 on the left top and right top panel respectively. The %VTEC vari-

ation during 17 March 2015 and 7 October 2015 on the left bottom and right bottom panel respectively

3.1 Positive response of diurnal variation of TEC to St. Patrick’s storm during 16 to 18 March 2015

Diurnal variation of IMF-Bz, Proton density, solar wind speed and dawn-dusk component of interplanetary electric field (Ey) are shown in Fig. 3. They represent the background solar, interplanetary and geophysical conditions for 16 to 18 March 2015. Figure 4 shows the evolution of storm time ring current intensity (SYM-H), AE, Kp Index and TEC variation over the observatory station from top to bottom panel respectively. Kataoka et al. (2015) shows that, a halo CME was detected on 15 March 2015 and high speed solar wind stream was traveling behind the CME from the large coronal hole. The variation of SYM-H shows that the geomagnetic storm occurred in two phases, first one was observed at 0800 UT with SYM-H magnitude of -91 nT and second phase was occurred around 2200 UT with SYM-H magnitude of -221 nT. The AE index has shown the significant enhancement on 17 March 2015 with magnitude of 2215 nT. This enhancement in the AE index during the episode of geomagnetic storm indicates the generation of energy source in the high latitude region, which produces

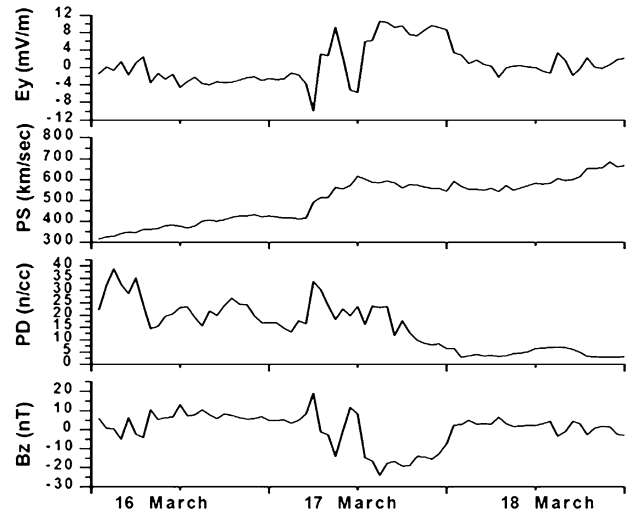


Fig. 3 Diurnal variation of IEF-Ey, Solar wind speed, Proton density and IMF-Bz on 16 March 2015 to 18 March 2015 from top to bottom panel

the equatorward wind and surges. The daytime westward and nighttime eastward Dynamo electric field is the results

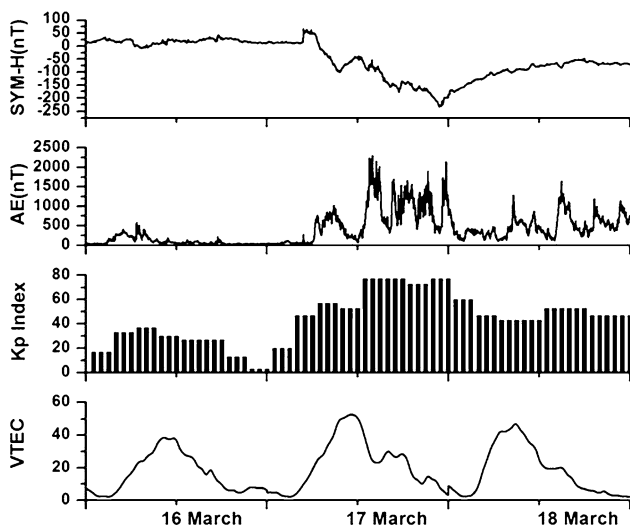


Fig. 4 Diurnal variation of Sym-H, AE index, Kp Index and VTEC on 16 March 2015 to 18 March 2015 from top to bottom panel

of equatorward winds and surges (Zhao et al. 2005; Kumar and Singh 2011).

The variation of VTEC also shows two step positive storm effects. First positive response of TEC was marked at 1000 UT with magnitude of 52.45 TECU and second positive response was noted around 1700 UT with magnitude of 27.32 TECU. The VTEC observed on 17 March 2015 is higher in magnitude as compared to its preceding and succeeding days (16 March and 18 March 2015). The short term positive response of the geomagnetic storm could be due to the traveling atmospheric disturbances (TADs) as suggested by Prölss and Jung (1978). TADs are the prior reason for positive ionospheric storm effect and geomagnetic activity effect at low latitude. Prölss (1993a,b) reported that these TADs originate from the high latitude regions and travel with high speed towards the mid and low latitude region. They are accompanied with meridional winds which could lift up the ionospheric F2 layer by many tens of kilometers in a span of half an hour or less.

Figure 5 shows that on 17 March 2015, the F2 layer critical frequency (foF2), its height (hmF2), and minimum virtual height of F2 layer (hF2) have increased after the trigger of storm and it can be seen that all three parameters get higher in magnitude as compared to average ten quiet days values. The enhancement in hmF2 started around 11:50 UT, after the first time trigger of the storm and persisted for a longer period of time. Zhang et al. (2015) also observed the positive response of St. Patrick's Day storm in terms of enhancement in foF2 and hmF2 over the low latitude region. The concentration of O⁺ ions starts increasing in the F2 layer due to lower recombination rate with simultaneous decrease in the concentration of N₂ resulting in the overall enhancement of O/N₂ ratio. The global hourly variation of O/N₂ ratio is shown in Fig. 6. The phenomena of the O/N₂

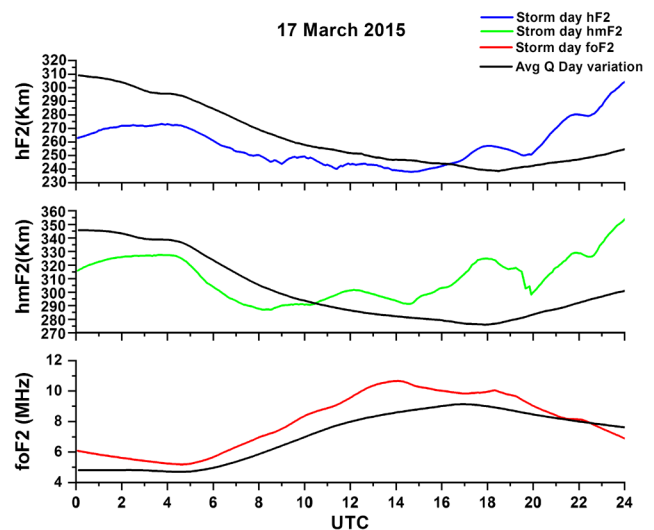


Fig. 5 Diurnal variation of hF2 (blue), hmF2 (green), and foF2 (red) and averaged ten quiet days of hF2, hmF2, and foF2 on 17 March 2015 from top to bottom panel

ratio enhancement during the positive storm effects is very well explained by the Burns et al. (1995), in which they have reported that Oxygen atom density shown enhancement by 50–60% while the Nitrogen molecules density are depleted by the 30–35% at the constant height surfaces. During the geomagnetic storm it is observed that there was rapid enhancement in the foF2 indicating participation of daytime prompt penetration electric field (PPEF). The PPEF is originated at the magnetospheric region and is mapped down to manifest the effects across the low latitude ionosphere. Sharma et al. (2012) reports instances of simultaneous experience of PPEF over a broad range of latitudes. Nava et al. (2016) also demonstrates occurrences of positive storm effect on ionosphere during the storm main phase over low altitudes and explaining the enhancement in TEC through the enhancement in hmF2. This could be due to the consequence of decreased recombination rate at higher altitudes (Prölss 1993a,b; Bauske and Prölss 1997).

3.2 Negative response of diurnal variation of TEC to the geomagnetic storm on 7 October 2015

Figure 7 shows the diurnal variation of interplanetary magnetic field (IMF-Bz), Proton density (PD), Solar wind speed (SW) and interplanetary electric field (Ey) from bottom to top panel respectively. The storm sudden commencement (SSC) was observed in two steps. First SSC was felt at 0500 UT with IMF-Bz magnitude of -8.45 nT (southward) and PD also showed a peak around 0300 UT with magnitude of 25.55 n/cc. While second SSC occurred around at 1500 UT with IMF Bz magnitude of -8.01 nT (southward) and PD of 28.8 n/cc at 1400 UT. The SW showed an enhancement exactly at 1400 UT with eastward electric field

Fig. 6 Hourly global variation of O/N2 from 1100 UT to 1400 UT on 17 March, 2015

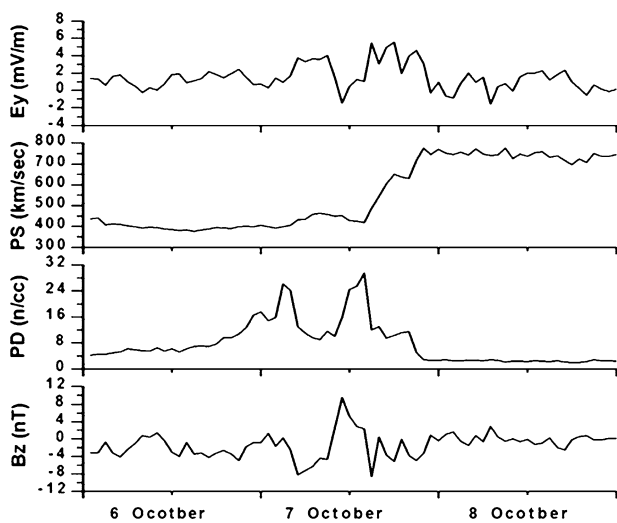
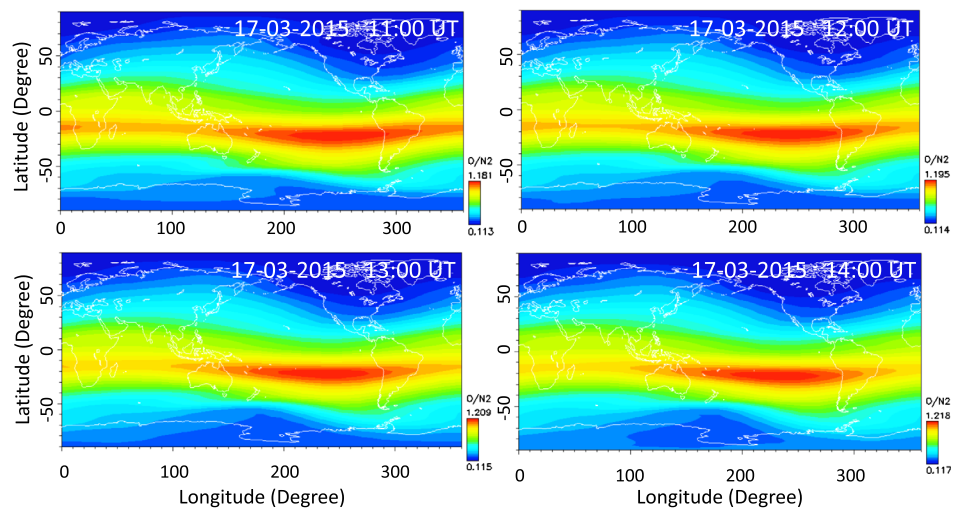


Fig. 7 Diurnal variation of IEF-Ey, Solar wind speed, Proton density and IMF-Bz on 6 October 2015 to 8 October 2015 from top to bottom panel

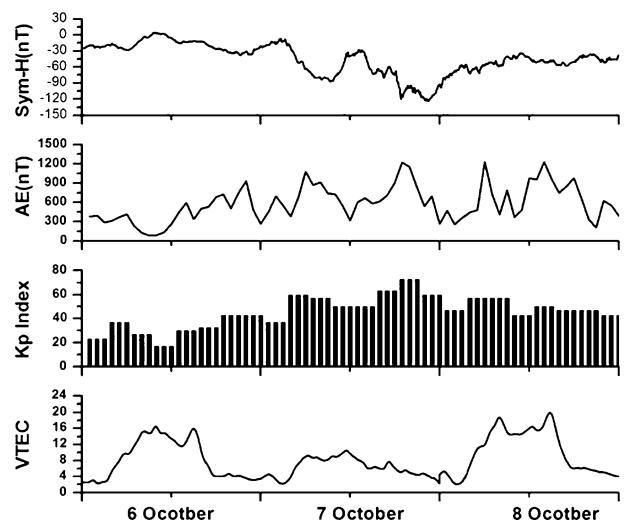


Fig. 8 Diurnal variation of Sym-H, AE index, Kp Index and VTEC on 6 October 2015 to 8 October 2015 from top to bottom panel

magnitude of 5.34 mV/meter. The IMF-Bz and IEF-Ey are very well correlated with eastward directed Ey during southward turning in Bz and vice versa.

Figure 8 depicts diurnal plot of Sym-H, AE, Kp index and diurnal variation of VTEC at the observatory station from top to bottom panel respectively. It can be observed from the Sym-H variation that the storm commenced around 0300 UT and 1300 UT and then the main phase of the storm at 1900 UT with magnitude of Sym-H -116.42 nT on 7 October 2015. The main phase of the geomagnetic storm persisted till early morning of 8 October 2015. The AE index indicates a significant enhancement from 2200 UT on 6 October 2015 where IMF-Bz first time went southward from northward direction and then AE index shows peak at 0500 UT and 1800 UT on 7 October 2015 with magnitude

of 1065.34 nT and 1209.30 nT respectively, during the storm main phase.

The VTEC gets depleted during the geomagnetic storm. The maximum value of VTEC was observed 16.01 TECU on 6 October 2015, while on the storm day the observed maximum VTEC was only 10 TECU, which indicated a negative ionospheric effect of geomagnetic storm. VTEC depletion started from the Storm commencement i.e., from the 2200 UT on 6 October 2015. The corresponding magnitude of VTEC during the storm main phase was very low on 7 October 2015 at the observatory station. The Ey field is westward on the storm commencement period with magnitude of 5.52 mV/meter and it inhibits the equatorial ionization anomaly (EIA) causing negative ionospheric effect. Studies of Kalita et al. (2016) reports the negative effect in the low latitude during the storm recovery phase attributing it to the inhibited EIA as well as modifications in the

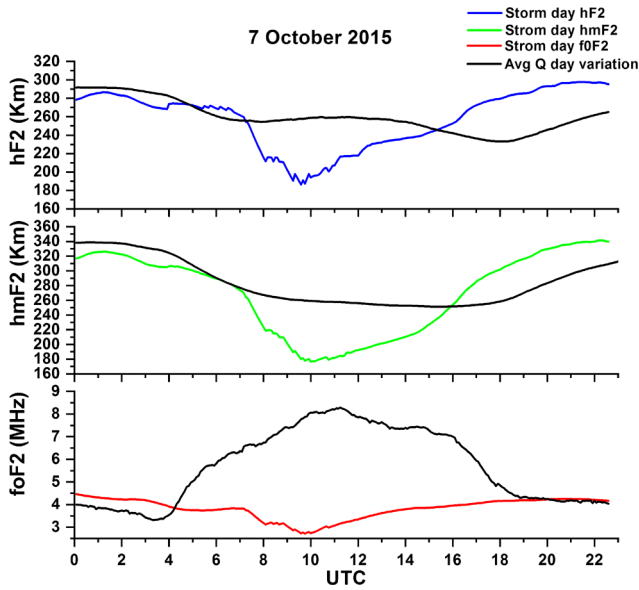


Fig. 9 Diurnal variation of hF2 (blue), hmF2 (green), and foF2 (red) and averaged ten quiet days of hF2, hmF2, and foF2 on 7 October 2015 from top to bottom panel

thermospheric composition. When the EIA inhibition region overlaps with the O/N2 depletion region to the low latitude region, it causes the negative ionospheric effect.

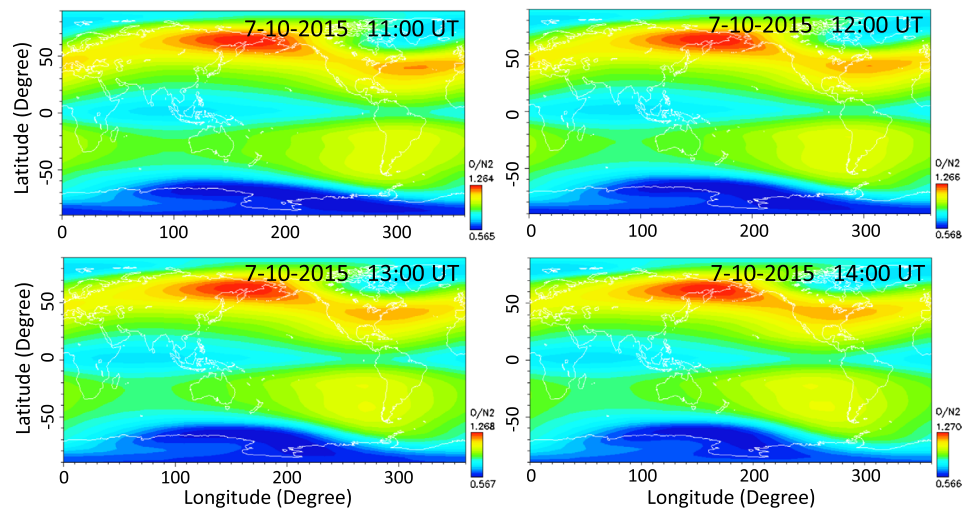
Figure 9 shows that on 7 October 2015, the F2 layer critical frequency (foF2), its height (hmF2), and minimum virtual height of F2 layer (hF2) are declined over the station after the storm triggered and the values of all three parameters shown the decrement with respect to averaged ten quiet day's values. This negative response of geomagnetic storm could be because of the downward $E \times B$ drift (i.e. depletion in hmF2) and depletion of O/N2 over the observatory region. The hmF2 depletion over the low latitude region is the combined effect of thermospheric neutral wind and O/N2 depletion. Figure 10 shows the global variation of O/N2 ratio on

7 October 2015 and it shows the O/N2 ratio is very much higher at northern hemisphere region and equatorial region as compared to the low latitude region. During the geomagnetic storm period O+ ions gets converted into NO+ due to the enhancement in the ion temperature. The conversion of O+ ion is very fast as compared to the O+ generation in the ionosphere, which leads to depletion in O/N2 ratio. Rishbeth et al. (1987) also explained that if O/O2 and O/N2 ratio shown depletion, it could cause decrement in the VTEC or could be the cause of negative ionospheric effect of storm.

3.3 Scintillation during both magnetic storm and their intercomparison

Figure 11 shows that scintillation is higher during the main phase and recovery phase of the St. Patrick's Day storm event on 17 March 2015. Scintillation was observed with peak value of S4 index (0.8) prior to the storm main phase. During the main phase of the storm, scintillation was intense (average S4 index was 0.6), frequent, and persistent till the recovery phase. Similarly, Fig. 12 shows that scintillation on 7 October 2015, Scintillation was observed prior to the main phase of the geomagnetic storm, on 6 October 2015 the S4 index was observed 0.72 and it continues till the recovery phase of the storm. The average value of the S4 index was 0.55 and frequency of scintillation was also higher during all the phases of geomagnetic storm, while highest S4 index value (0.75) was observed during the main phase of the storm. The scintillation is produced by the developed ionospheric irregularities. The irregularities developed at low latitude region are observed at irregular intervals and as it moves towards the equatorial region the time span of the irregularity increases. The mechanism of development of ionospheric irregularities frequently over the low latitudes can be described in terms of ion neutral collision frequency, gravity wave, large scale plasma gradient, neutral wind etc.

Fig. 10 Hourly global variation of O/N2 from 1100 UT to 1400 UT on 7 October, 2015



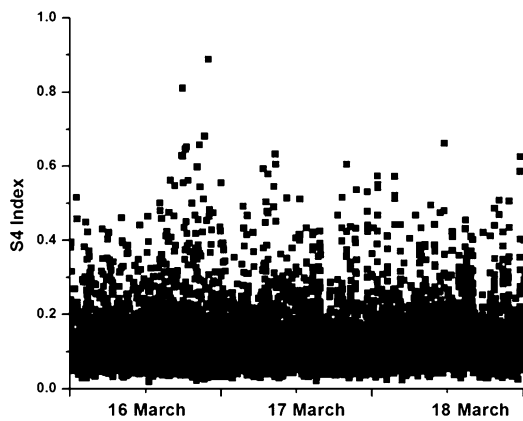


Fig. 11 Diurnal variation of Scintillation (S4 index) in the form of scatter plot on 16 March 2015 to 18 March 2015

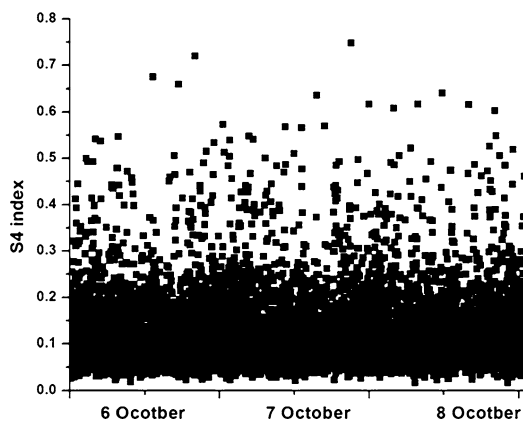


Fig. 12 Diurnal variation of Scintillation (S4 index) in the form of scatter plot on 6 October 2015 to 8 October 2015

Li et al. (2007) explained that during the geomagnetic storm, eastward electric field enhances and forces to move the plasma by the $E \times B$ drift, which results in the Rayleigh–Taylor instability, manifesting plasma bubbles and spread-F irregularities that are responsible for scintillations in the radio signals.

The enhanced scintillation during the St. Patrick’s Day storm was the combined effect of enhanced neutral density and traveling atmospheric disturbances over low latitude and equatorial region. The intensity of the scintillation (S4 index) would be higher around the EIA crest region, because in the EIA crest region plasma moves from the low latitude to equatorial region accompanying the thermospheric neutral wind, which produces the plasma density gradient. During the 7 October geomagnetic storm height of F layer decreases, which sparse a scintillation occurrence. If the storm occurs at the day time, the scintillation is weak during the main phase as well as the recovery phase, due to the sudden generation of DDEF (Basu et al. 2001) but if the storm occurs during the early morning time or post-midnight time (as in the case of 7 October 2015), the scintillation will be higher during the main and recovery phases of the storm.

4 Conclusion

The diurnal variation of ionospheric TEC during the St. Patrick’s Day storm and during the 7 October 2015 has been investigated through GPS-TEC observations over the RASH station (28°29’N, 34°46’E). The Scintillation generated over the observatory station due to the effect of geomagnetic storms has been also investigated and shows some interesting results. The major result of the study as follows:

- (i) The positive ionospheric response to the St. Patrick’s Day storm may be caused by the combined effect of traveling atmospheric disturbances (TADs) and Prompt penetration electric field (PPEF) while the disturbance dynamo electric field was in progress for an extended period.
- (ii) The negative ionospheric response to the geomagnetic storm of 7 October 2015 corresponds to the downward movement of plasma due to the suppressed $E \times B$ drift and inhibited equatorial ionization anomaly (EIA).
- (iii) The scintillation generated during the geomagnetic storms could be the result of development of plasma bubbles and spread-F irregularities over the low latitude region.

The investigation of severe and strong geomagnetic storms during two different equinoctial seasons over the low latitude Saudi Arabia region has been performed to strengthen the understanding on ionospheric variability over the region. The study complements a global effort towards clearer understanding and modeling of ionospheric variability and delay error associated with the transionospheric satellite communication, navigation and timing applications.

Acknowledgements The authors extend their appreciation to the Deanship of Scientific Research at Majmaah University for funding this work under project number (RGP-2019-25). The authors would like to thank Community Coordinated Modeling Center (CCMC), NASA Goddard Space Flight Center for providing O/N₂ data. The authors would like to thank Global Ionosphere Radio Observatory for providing the F region parameters (hmF2, foF2 and hF2) from ionosonde station Athens (38°N, 23°E). The authors thank Gopi Seemala for providing access to the Rinex GPS-TEC program to determine the VTEC GNSS observations. The authors also acknowledge OMNI Web Data Explorer and World Data Centre Kyoto for availing the solar, geophysical and magnetic parameters.

Publisher’s Note Springer Nature remains neutral with regard to jurisdictional claims in published maps and institutional affiliations.

References

- Ansari, K., Park, K.D., Panda, S.K.: Empirical Orthogonal Function analysis and modeling of ionospheric TEC over South Korean region. *Acta Astronaut.* **161**, 313–324 (2019)
- Araki, T., Allen, J.H., Araki, Y.: Extension of a polar ionospheric current to the nightside equator. *Planet. Space Sci.* **33**(1), 11–16 (1985)

- Astafyeva, E., Zakharenkova, I., Förster, M.: Ionospheric response to the 2015 St. Patrick's Day storm: a global multi-instrumental overview. *J. Geophys. Res. Space Phys.* **120**(10), 9023–9037 (2015)
- Basu, S., Basu, S., Valladares, C.E., Yeh, H.C., Su, S.Y., MacKenzie, E., Sultan, P.J., Aarons, J., Rich, F.J., Doherty, P., Groves, K.M.: Ionospheric effects of major magnetic storms during the International Space Weather Period of September and October 1999: GPS observations, VHF/UHF scintillations, and in situ density structures at middle and equatorial latitudes. *J. Geophys. Res. Space Phys.* **106**(A12), 30389–30413 (2001)
- Bauske, R., Pröls, G.W.: Modeling the ionospheric response to traveling atmospheric disturbances. *J. Geophys. Res. Space Phys.* **102**(A7), 14555–14562 (1997)
- Blanc, M., Richmond, A.D.: The ionospheric disturbance dynamo. *J. Geophys. Res. Space Phys.* **85**(A4), 1669–1686 (1980)
- Borries, C., Mahrous, A.M., Ellahouy, N.M., Badeke, R.: Multiple ionospheric perturbations during the Saint Patrick's Day storm 2015 in the European-African sector. *J. Geophys. Res. Space Phys.* **121**(11), 11–333 (2016)
- Burns, A.G., Killeen, T.L., Carignan, G.R., Roble, R.G.: Large enhancements in the O/N2 ratio in the evening sector of the winter hemisphere during geomagnetic storms. *J. Geophys. Res. Space Phys.* **100**(A8), 14661–14671 (1995)
- Carter, B.A., Yizengaw, E., Pradipta, R., Retterer, J.M., Groves, K., Valladares, C., Caton, R., Bridgwood, C., Norman, R., Zhang, K.: Global equatorial plasma bubble occurrence during the 2015 St. Patrick's Day storm. *J. Geophys. Res. Space Phys.* **121**(1), 894–905 (2016)
- Chen, C.H., Lin, C.H., Matsuo, T., Chen, W.H.: Ionosphere data assimilation modeling of 2015 St. Patrick's Day geomagnetic storm. *J. Geophys. Res. Space Phys.* **121**(11), 11–549 (2016)
- De Jesus, R., Sahai, Y., Guarnieri, F.L., Fagundes, P.R., De Abreu, A.J., Bittencourt, J.A., Nagatsuma, T., Huang, C.S., Lan, H.T., Pillat, V.G.: Ionospheric response of equatorial and low latitude F-region during the intense geomagnetic storm on 24–25 August 2005. *Adv. Space Res.* **49**(3), 518–529 (2012)
- Goncharenko, L.P., Foster, J.C., Coster, A.J., Huang, C., Aponte, N., Paxton, L.J.: Observations of a positive storm phase on September 10, 2005. *J. Atmos. Sol.-Terr. Phys.* **69**(10–11), 1253–1272 (2007)
- Hairston, M., Coley, W.R., Stoneback, R.: Responses in the polar and equatorial ionosphere to the March 2015 St. Patrick Day storm. *J. Geophys. Res. Space Phys.* **121**(11), 11–213 (2016)
- Huang, C.S., Foster, J.C., Kelley, M.C.: Long-duration penetration of the interplanetary electric field to the low-latitude ionosphere during the main phase of magnetic storms. *J. Geophys. Res. Space Phys.* **110**, A11309 (2005)
- Huang, C.S., Sazykin, S., Chau, J.L., Maruyama, N., Kelley, M.C.: Penetration electric fields: efficiency and characteristic time scale. *J. Atmos. Sol.-Terr. Phys.* **69**(10–11), 1135–1146 (2007)
- Kalita, B.R., Hazarika, R., Kakoti, G., Bhuyan, P.K., Chakrabarty, D., Seemala, G.K., Wang, K., Sharma, S., Yokoyama, T., Supnithi, P., Komolmis, T.: Conjugate hemisphere ionospheric response to the St. Patrick's Day storms of 2013 and 2015 in the 100°E longitude sector. *J. Geophys. Res. Space Phys.* **121**(11), 11–364 (2016)
- Kataoka, R., Shiota, D., Kilpua, E., Keika, K.: Pileup accident hypothesis of magnetic storm on 17 March 2015. *Geophys. Res. Lett.* **42**(13), 5155–5161 (2015)
- Kikuchi, T.: Evidence of transmission of polar electric fields to the low latitude at times of geomagnetic sudden commencements. *J. Geophys. Res. Space Phys.* **91**(A3), 3101–3105 (1986)
- Kikuchi, T., Araki, T.: Horizontal transmission of the polar electric field to the equator. *J. Atmos. Terr. Phys.* **41**(9), 927–936 (1979)
- Kikuchi, T., Hashimoto, K.K.: Transmission of the electric fields to the low latitude ionosphere in the magnetosphere-ionosphere current circuit. *Geosci. Lett.* **3**(1), 4 (2016)
- Kikuchi, T., Hashimoto, K.K., Nozaki, K.: Penetration of magnetospheric electric fields to the equator during a geomagnetic storm. *J. Geophys. Res. Space Phys.* **113**, A06214 (2008)
- Kil, H., Lee, W.K., Paxton, L.J., Hairston, M.R., Jee, G.: Equatorial broad plasma depletions associated with the evening prereversal enhancement and plasma bubbles during the 17 March 2015 storm. *J. Geophys. Res. Space Phys.* **121**(10), 10–209 (2016)
- Koba, A.T., Richmond, A.D., Emery, B.A., Peymirat, C., Lühr, H., Moretto, T., Hairston, M., Amory-Mazaudier, C.: Electrodynamic coupling of high and low latitudes: observations on May 27, 1993. *J. Geophys. Res. Space Phys.* **105**(A10), 22979–22989 (2000)
- Kumar, S., Singh, A.K.: Storm time response of GPS-derived total electron content (TEC) during low solar active period at Indian low latitude station Varanasi. *Astrophys. Space Sci.* **331**(2), 447–458 (2011)
- Li, G., Ning, B., Liu, L., Ren, Z., Lei, J., Su, S.-Y.: The correlation of longitudinal/seasonal variations of evening equatorial prereversal drift and of plasma bubbles. *Ann. Geophys.* **25**, 2571–2578 (2007). <https://doi.org/10.5194/angeo-25-2571-2007>
- Lu, G., Goncharenko, L.P., Richmond, A.D., Roble, R.G., Aponte, N.: A dayside ionospheric positive storm phase driven by neutral winds. *J. Geophys. Res. Space Phys.* **113**, A08304 (2008)
- Nava, B., Rodríguez-Zuluaga, J., Alazo-Cuartas, K., Kashcheyev, A., Migoya-Orué, Y., Radicella, S.M., Amory-Mazaudier, C., Fleury, R.: Middle-and low-latitude ionosphere response to 2015 St. Patrick's Day geomagnetic storm. *J. Geophys. Res. Space Phys.* **121**(4), 3421–3438 (2016)
- Panda, S.K., Gedam, S.S., Rajaram, G., Sripathi, S., Pant, T.K., Das, R.M.: A multi-technique study of the 29–31 October 2003 geomagnetic storm effect on low latitude ionosphere over Indian region with magnetometer, ionosonde, and GPS observations. *Astrophys. Space Sci.* **354**(2), 267–274 (2014)
- Pröls, G.W.: January. On explaining the local time variation of ionospheric storm effects. *Ann. Geophys.* **11**, 1–9 (1993a)
- Pröls, G.W.: Common origin of positive ionospheric storms at middle latitudes and the geomagnetic activity effect at low latitudes. *J. Geophys. Res. Space Phys.* **98**(A4), 5981–5991 (1993b)
- Pröls, G.W., Jung, M.J.: Travelling atmospheric disturbances as a possible explanation for daytime positive storm effects of moderate duration at middle latitudes. *J. Atmos. Terr. Phys.* **40**(12), 1351–1354 (1978)
- Reddybattula, K.D., Panda, S.K.: Performance analysis of quiet and disturbed time ionospheric TEC responses from GPS-based observations, IGS-GIM, IRI-2016 and SPIM/IRI-Plas 2017 models over the low latitude Indian region. *Adv. Space Res.* **64**(10), 2026–2045 (2019)
- Reddybattula, K.D., Panda, S.K., Ansari, K., Peddi, V.S.R.: Analysis of ionospheric TEC from GPS, GIM and global ionosphere models during moderate, strong, and extreme geomagnetic storms over Indian region. *Acta Astronaut.* **161**, 283–292 (2019)
- Richmond, A.D., Roble, R.G.: Dynamic effects of aurora-generated gravity waves on the mid-latitude ionosphere. *J. Atmos. Terr. Phys.* **41**(7–8), 841–852 (1979)
- Rishbeth, H., Fuller-Rowell, T.J., Rees, D.: Diffusive equilibrium and vertical motion in the thermosphere during a severe magnetic storm: a computational study. *Planet. Space Sci.* **35**(9), 1157–1165 (1987)
- Sahai, Y., Fagundes, P.R., de Jesus, R., de Abreu, A.J., Crowley, G., Kikuchi, T., Huang, C.-S., Pillat, V.G., Guarnieri, F.L., Abalde, J.R., Bittencourt, J.A.: Studies of ionospheric F-region response in the Latin American sector during the geomagnetic storm of 21–22 January 2005. *Ann. Geophys.* **29**, 919–929 (2011)
- Seemala, G.K., Valladares, C.E.: Statistics of total electron content depletions observed over the South American continent for the year 2008. *Radio Sci.* **46**, RS5019 (2011)

- Seif, A., Abdullah, M., Hasbi, A.M., Zou, Y.: Investigation of ionospheric scintillation at UKM station, Malaysia during low solar activity. *Acta Astronaut.* **81**(1), 92–101 (2012)
- Sharma, S.K.: Ionospheric TEC variation over Manama, Bahrain and comparison with NeQuick-2 model. *Astrophys. Space Sci.* **364**, 16 (2019)
- Sharma, S., Galav, P., Dashora, N., Dabas, R.S., Pandey, R.: Study of ionospheric TEC during space weather event of 24 August 2005 at two different longitudes. *J. Atmos. Sol.-Terr. Phys.* **75**, 133–140 (2012)
- Sharma, S.K., Ansari, K., Panda, S.K.: Analysis of ionospheric TEC variation over Manama, Bahrain, and comparison with IRI-2012 and IRI-2016 models. *Arab. J. Sci. Eng.* **43**(7), 3823–3830 (2018)
- Somayajulu, V.V., Reddy, C.A., Viswanathan, K.S.: Penetration of magnetospheric convective electric field to the equatorial ionosphere during the substorm of March 22, 1979. *Geophys. Res. Lett.* **14**(8), 876–879 (1987)
- Yamazaki, Y., Kosch, M.J.: The equatorial electrojet during geomagnetic storms and substorms. *J. Geophys. Res. Space Phys.* **120**(3), 2276–2287 (2015)
- Zhang, S.R., Erickson, P.J., Foster, J.C., Holt, J.M., Coster, A.J., Makela, J.J., Noto, J., Meriwether, J.W., Harding, B.J., Riccobono, J., Kerr, R.B.: Thermospheric poleward wind surge at midlatitudes during great storm intervals. *Geophys. Res. Lett.* **42**(13), 5132–5140 (2015)
- Zhao, B., Wan, W., Liu, L.: Responses of equatorial anomaly to the October–November 2003 superstorms. *Ann. Geophys.* **23**(3), 693–706 (2005)
- Zhou, Y.L., Lüher, H., Xiong, C., Pfaff, R.F.: Ionospheric storm effects and equatorial plasma irregularities during the 17–18 March 2015 event. *J. Geophys. Res. Space Phys.* **121**(9), 9146–9163 (2016)